Internal Report #77

CRS LET Detector Thickness, Area and Geometry Factor Measurments

N. Gehrels and A. C. Cummings

November 1980

Table of Contents

I. Introduction

This report documents the thickness and area tests of the LET detectors on the Voyager CRS experiment. For reference Figure I-1 shows a schematic of a nominal LET telescope.

II. LET 35 Thickness Measurements

The thickness of each LET 35 μm detector was determined by measuring the energy loss of normally incident, penetrating α-particles from a ^{228}Th source (see Figure II-1 and Figure II-2a). The data and analysis are in the notebook labeled: "LET - 35 μm Dectectors - Particle Thickness Data".

Each raw data set consisted of 11 pulse height spectra. For pulse height spectra 4 and 6-9, all but an annular ring of the detector was masked off so that thickness measurements could be made at various distances from the center (see Figure II-2b). The inner and outer radii of the exposed annular area for these runs are listed on the third page of each data set. The other six pulse height spectra were taken for special purposes as follows:

nos. 1,2,10,11	-	pulser calibrations of the electronics before and after each complete set of spectra
no. 5	-	a measurement with the detector at half bias
no. 3	-	a measurement with all but an r = 1 mm hole masked off to determine the Landau contribution to the sigma of the other thickness distributions

The raw data for all spectra are listed and plotted on pages five through ten of

each data set. Calculations to obtain an average thickness and an average path length for an isotropic flux (L1-L2 required) are shown on page three.

To determine the average secant ϑ of an isotropic flux for each annular ring, it was necessary to numerically intergrate over acceptable solid angles. Plots of the secant ϑ distributions, as well as listings of all programs involved in this thickness determination are in the "Analysis" section of the notebook. The final results for all flight detectors are listed in Table VIII.

III. LET 450 Thickness Measurements

The thickness of each 450 μm detector at a point on its surface was determined by comparison with a gaugeblock of known thickness (457.2 μm). The data and analysis are in the notebook labeled: "LET - 450 μm Detectors - Thickness Data, Depletion Voltage Data".

The two sides of a detector (or gaugeblock) were shorted and the surface was pulsed. Probes were then brought near both sides of the detector (gaugeblock) causing pulses to be capacitively induced in them. By adjusting the probe - surface distance, d, so that the ratio of the number of output pulse above some threshold to input pulses, $\frac{O}{I}$, was one half, a fixed d could be obtained (see Figure III-1). The actual measurements were done as follows: A probe - gaugeblock - probe "sandwich" was formed with one probe fixed. The gaugeblock was pulsed, and its position was adjusted until $\left[\frac{O}{I}\right]_{fixed} = 0.5$. Next, the position of the free probe was adjusted until $\left[\frac{O}{I}\right]_{free} = 0.5$. The probe - surface distance on both sides of the guageblock was thus set. The gaugeblock was then replaced by the detector of unknown thickness, $T_{detector}$. The detector was now pulsed and its position adjusted until $\left[\frac{O}{I}\right]_{fixed} = 0.5$, thereby

reproducing the fixed probe - surface distance of the gaugeblock run. Finally, the free probe was moved a distance Δ such that $\left[\frac{O}{I}\right]_{free} = 0.5$, reproducing the free probe - surface distance of the gaugeblock run. Therefore, as shown in Figure III-2:

$$T_{detector} = 457.2\ \mu m - \Delta\ .$$

Two measurements at the center of the detector were averaged to give T_{center}; measurements at four positions around the edge were averaged to give T_{edge}. All numbers can be found in the "Data" section of the notebook. By comparing the two measurements at the center of each detector the rms uncertainty on each thickness measurement is estimated to be 1.7 μm

In order to calculate the average thickness and path length of a detector, it was necessary to know its shape. Since all the 450 μm detectors measured were found to have $T_{center} > T_{edge}$, it was assumed as a first approximation that the two sides were identical spherical sections (see Figure III-3a) so that:

$$T(r) = T_{center} - (T_{center} - T_{edge}) \frac{r^2}{r^2_{edge}} \qquad (1)$$

where r_{edge} = 8 mm, is the distance from the center of the detector to the position at which T_{edge} was measured (see Figure III-3b). This relation is derived in the "Analysts" section of the notebook. Using equation (1), the average thickness was easily determined. In order to approximate the average particle path length for an isotropic flux (L1-L2 required), the detector was divided into several annular rings. The average detector thickness for each annular area was determined using equation (1), and the average secant ϑ for each area was computed by the program RINGSPLT. The product was then averaged over all annular rings weighted by geometry factor to give the average path length. The result is slightly dependent on whether the detector is an L3 or an L4 detector.

This analysis, as well as a listing of RINGSPLT, is in the "Analysis" section of the notebook. The average thicknesses and path lengths for all flight detectors are listed

in Tables I and II.

IV. LET 35 Active Area Measurements

The active area of each 35 μm detector was determined by counting the total number of stopping α-particles from a ^{241}Am source in a constant time, and then comparing to the standard detector, 15-158C (see Figure IV-1). The data, program listings and analysis are in the notebook labeled "LET 35 μm Detectors - Particle Area Data, Optical Size Scans, Testing Charts, Warranties".

The data for each detector are made up of a pulser calibration of the electronics at 0.5, 2 and 5 MeV and a pulse-height analysis spectrum of the detector's output during a 400 second exposure to the source. The calibration analysis was done using the program DETAREA (see notebook). The various detectors were run in groups on several different days. Each group run included a measurement of 15-158C as a standard. The pulse-height analysis spectra were similar for all detectors and can best be described by considering three energy regions:

< 2 MeV	variable tail due to background and extreme edge effects
2 - 4.9 MeV	flat nonvarying tail due to poor energy collection near the edge of the detector
4.9 - 5.7 MeV	α peak (~5.5 MeV); the spectra fall off more steeply for E > 5.5 MeV than for E < 5.5 MeV.

The total number of counts above 4.9 MeV was used to obtain the fully active area of each detector relative to the optical area of the standard detector, 15-158C. The results are listed in Table VII.

The lower limit of 4.9 MeV is ~10% below the nominal incident α energy and is intended to approximate a limit that might be used in real data analysis, for example separating α-particles from protons on a $\frac{dE}{dx}$-E plot. The summation was also perfomed for all channels above 2 MeV as a consistency check. Three items of concern were found in the data:

1) The pulse-height spectrum of the standard detector, 15-158C, on 4/14/76 is 20% below average. It is suspected that the run time was less than the normal 400 seconds.

2) There was a problem with the electronic calibration on 6/28/76. The spectra look normal, however, and could possibilty be integrated using the α peak to aid in the calibration. The data was not analyzed since it did not include any flight detectors.

3) The detectors run on 4/06/76 were rerun on 4/23/76, because of suspected problems. The data sets are reasonably consistent, but only the latter run was used in the final analysis.

There were a total of six runs used in the final analysis. The number of counts above 4.9 MeV for detector 15-158C for these runs is listed in Table IV-1.

Table IV-1

date	N (integrated counts)
3/17/76	673523
4/16/76	673591
4/21/76	673032
4/23/76	674978
4/28/76	675071
4/30/76	673049

The sample is small, but if a statistical distribution is assumed, $\overline{N} = 673874$ and $\frac{\sigma_N}{\overline{N}} = 0.14 \pm 0.04$ %. The relative sigma is consistent with counting statistics, $\frac{\sqrt{\overline{N}}}{\overline{N}} = 0.12$ %. $\overline{N}$ was therefore used as the standard for comparison with the results of other detectors.

Prior to these active-area measurements, a metallization goodness number had been assigned to most detectors as an aid in flight detector selection. The numbers ranged from one to six and were determined by optical inspection of the Au metallization as follows:

1 - distinct edge

.

.

6 - hazy edge, implying a thin metallization near the edge

Figure IV-2 is a plot of this number vs. the relative active area for all detectors that were inspected. As expected, there is a correlation between thin metallization regions and reduced active areas.

Another check on the reliability of the active-area measurement technique was made by redoing two detectors with different equipment and setup, approximately one year later. The results are listed in Table IV-2.

Table IV-2

detector	1976 measurement $\frac{\text{(detector area − 15−158C area)}}{\text{15−158C area}}$	1977 measurement $\frac{\text{(detector area − 15−158C area)}}{\text{15−158C area}}$
414-734 B	-2.79 ± 0.13%	-2.52 ± 0.04%
514-546 E	0.40 ± 0.13%	0.43 ± 0.04%

Finally, the active areas were used to calculate the relative geometry factors for all LET flight telescopes. These are listed in Table VIII. The L1-L2 separation distance was calculated from numbers in the LET assembly data notebooks. The error analysis can be found in the "Analysis" section of the notebook containing the area data.

V. LET 35 Optical Area Measurements

The optical area of each 35 μm detector was determined by measuring its diameter using a microscope with a calibrated scan platform. The data are in the notebook labeled "LET 35 μm Detectors - Particle Area, Optical Size Scans, Testing Charts, Visual Inspections Warranties".

Two diameters of the metallization, d_x and d_y, were measured in perpendicular directions on both the Au and Al sides of the detector. The area of each side was then:

$$A = \pi \frac{d_x}{2} \frac{d_y}{2} \quad .$$

Figure V-1a is a plot of the Au area vs. the Al area for all detectors.

A measurement was also made of the concentricity (distance between centers) of the Lavite mounting ring and the metallization on both sides. Unfortunately the absolute concentricity between the Au and Al metallizations could not be determined. In an effort to find out if the masking procedure during production caused similar concentricities in the same direction on both sides, a plot was made of the concentricity on the Al side vs. the concentricity on the Au side (see Figure V-1b). The concentricities did not seem well correlated and we were therefore forced to assume that, as a worst case, the maximum absolute concentricity could be the sum of the concentricities on the two sides.

The final optical areas of the Al side for all flight detectors are listed in Table VII.

Numbers in parenthesis are the areas of overlap of the Au and Al metallizations computed assuming the worst-case absolute concentricity.

VI. LET 450 Optical Area Measurements

The optical areas of the 450 μm detectors were measured in the same way as those of the 35 μm detectors (see Section V). The data are in the notebook labeled "LET - 450 μm Detectors - Optical Size Scans, Testing Charts, Visual Inspections, Warranties".

For these detectors, the concentricities of the metallizations were not measured. Table VII lists the epoxy-free optical areas for all flight 450 μm detectors.

Table VII

(FU-1, VGR 1)

Detector		Serial Number	Thickness (mean ± σ)ϕ	Average Path Length* (mean ± σ)ϕ	Optical Area L1,L2 (Al-(overlap)) L3,L4 (epoxy free)	Active Area**
LET A						
(09)†	L1	14-297B	36.98± 0.26 μm	37.91± 0.66 μm	2.834 - (2.80) cm^2	2.8384 cm^2
	L2	14-629D	34.60± 0.42	35.46± 0.82	2.832 - (2.81)	2.8259
	L3	14-773E	396.4 ±14.6	409.3 ±13.2	3.890	-
	L4	15-558B	450.8 ± 5.8	463.0 ± 9.0	4.071	-
LET B						
(13)	L1	14-631D	30.16± 0.24	30.91± 0.64	2.839 - (2.81)	2.8228
	L2	14-546C	37.58± 0.63	38.51± 0.99	2.841 - (2.82)	2.8466
	L3	14-773F	386.2 ±12.2	398.3 ±11.5	3.878	-
	L4	15-561F	449.2 ±11.2	462.3 ±11.5	4.102	-
LET C						
(07)	L1	14-630C	36.17± 0.61	37.07± 0.98	2.839 - (2.81)	2.8273
	L2	14-544C	32.26± 0.28	33.07± 0.63	2.838 - (2.82)	2.8222
	L3	14-295I	397.1 ±24.2	411.9 ±21.0	3.871	-
	L4	15-721H	451.4 ± 9.7	464.4 ±10.6	4.108	-
LET D						
(16)	L1	14-548E	34.58± 0.49	35.45± 0.72	2.831 - (2.81)	2.8112
	L2	14-548D	33.82± 0.46	34.66± 0.80	2.831 - (2.82)	2.8152
	L3	14-772A	400.7 ±17.4	414.8 ±15.1	3.958	-
	L4	15-796G	464.3 ± 7.2	477.1 ± 9.7	4.053	-

ϕ σ is the rms deviation of the thickness (pathlength) distribution.

* Isotropic Flux; L1·L2 required.

** The relative accuracy of these areas is ±0.0037 cm^2 compared to the assumed area of 15-158C of 2.82932 cm^2 (only absolutely known to a few percent).

† Telescope Serial Number.

Table VII cont.

(FU-2, VGR 2)

Detector		Serial Number	Thickness (mean ± σ)§	Average Path Length* (mean ± σ)§	Optical Area L1,L2 (Al-(overlap)) L3,L4 (epoxy free)	Active Area**
LET A						
(11)†	L1	14-541D	33.53± 0.65 μm	34.35± 1.03 μm	2.837 - (2.81) cm^2	2.8180 cm^2
	L2	14-544A	35.34± 0.51	36.23± 0.72	2.834 - (2.81)	2.8299
	L3	15-796I	447.9 ± 8.5	461.2 ± 7.2	3.985	-
	L4	15-720G	448.6 ± 9.7	461.2 ±10.7	4.034	-
LET B						
(15)	L1	15-164C	37.62± 0.32	38.55± 0.81	2.831 - (2.81)	2.8064
	L2	14-541E	29.93± 0.48	30.67± 0.81	2.835 - (2.82)	2.8251
	L3	14-294E	412.4 ±22.3	428.0 ±18.9	3.969	-
	L4	15-561H	453.5 ± 9.5	466.3 ±10.5	4.065	-
LET C						
(10)	L1	14-546B	34.47± 0.57	35.33± 0.97	2.832 - (2.79)	2.8364
	L2	15-164D	33.21± 0.39	34.04± 0.77	2.834 - (2.82)	2.7900
	L3	15-717F	460.9 ±11.5	475.2 ±11.4	3.984	-
	L4	15-796E	445.1 ±10.3	457.5 ±10.9	4.006	-
LET D						
(14)	L1	14-544D	33.90± 0.41	34.76± 0.65	2.842 - (2.81)	2.8344
	L2	14-455D	35.33± 0.50	36.21± 0.92	2.832 - (2.81)	2.8039
	L3	14-771D	393.9 ±21.7	408.5 ±18.6	3.923	-
	L4	15-558F	441.6 ± 4.2	453.3 ± 8.8	4.083	-

* Isotropic Flux; L1·L2 required.

** The relative accuracy of these areas is ±0.0037 cm^2 compared to the assumed area of 15-158C of 2.82932 cm^2 (only absolutely known to a few percent).

† Telescope Serial Number.

§ σ is the rms deviation of the thickness (pathlength) distribution.

Table VIII

	L1 Active Area* (±0.0037 cm^2)	L2 Active Area (±0.0037 cm^2)	L1-L2 Separation (±0.005 cm)	$A\Omega$ ** (±0.0012 cm^2-sr)
FU-1				
LET A	2.8384 cm^2	2.8259 cm^2	4.076 cm	0.4366 cm^2-sr
LET B	2.8228	2.8466	4.081	0.4364
LET C	2.8273	2.8222	4.079	0.4338
LET D	2.8112	2.8152	4.075	0.4312
FU-2				
LET A	2.8180	2.8299	4.075	0.4344
LET B	2.8064	2.8251	4.064	0.4341
LET C	2.8364	2.7900	4.084	0.4295
LET D	2.8344	2.8039	4.061	0.4357

* Area relative to the optical area of 15-158C (2.82932 cm^2); see comment for Table VII.

** L1·L2 required; fourth place accuracy is only relative.

detector	thickness	radius
-	3 μm Al	-
L1	35 μm Si	0.95 cm
L2	35 μm Si	0.95 cm
L3	450 μm Si	1.13 cm
L4	450 μm Si	1.13 cm

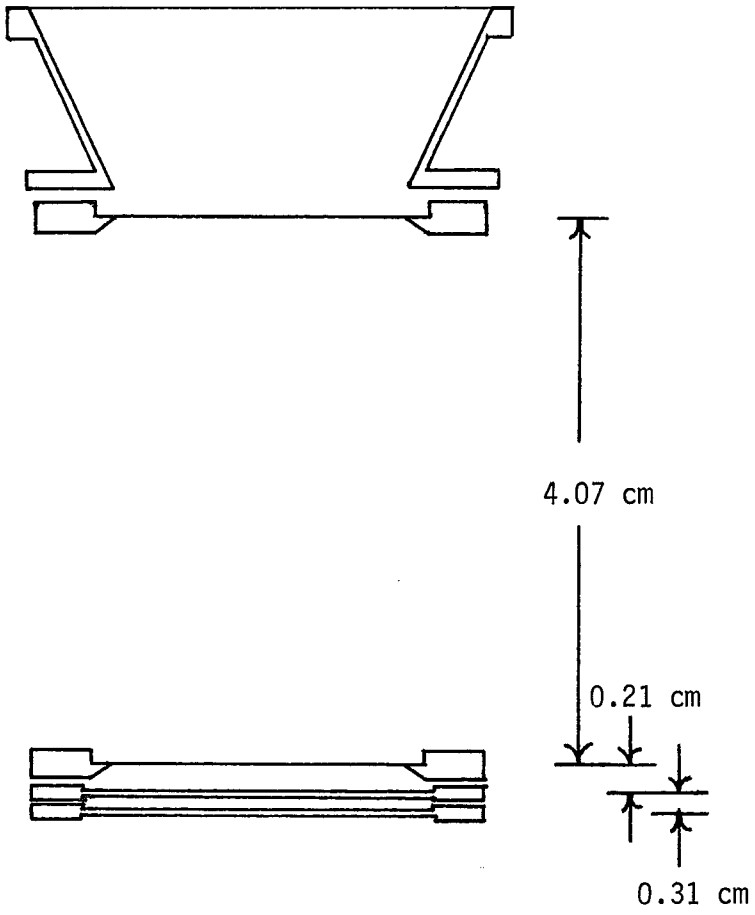

Nominal LET Telescope

Figure I-1

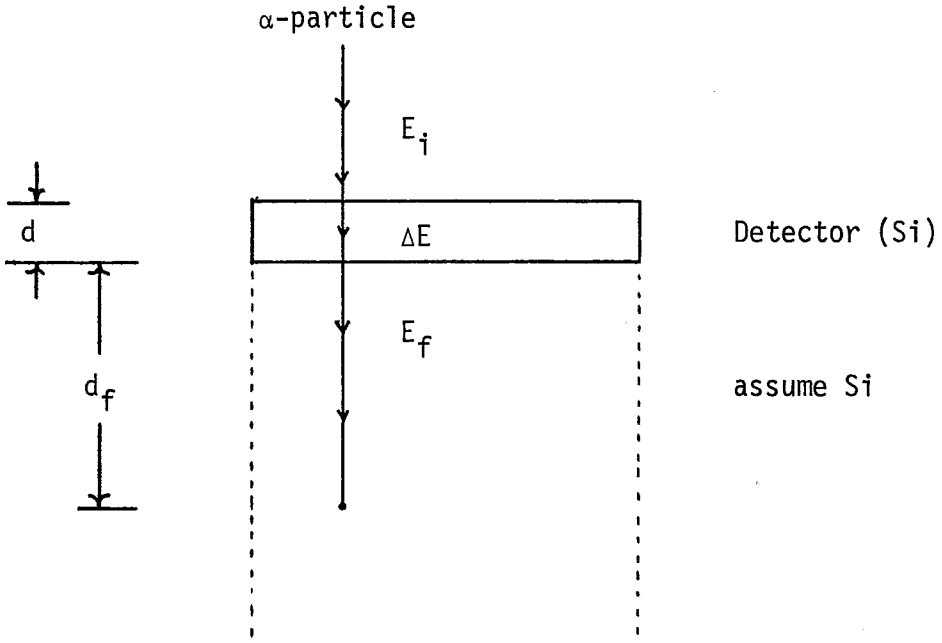

ILLUSTRATIVE CALCULATION

E_i and ΔE are known; d is to be determined.

$$R_\alpha(E_f) = d_f$$

$$R_\alpha(\Delta E + E_f) = d + d_f$$

where $R_\alpha(E)$ is the range in silicon of an α-particle of energy E (S. Vidor's range energy table was used).

Solving for d with $E_f = E_i - \Delta E$:

$$d = R_\alpha(E_i) - R_\alpha(E_i - \Delta E)$$

Figure II-1

a)

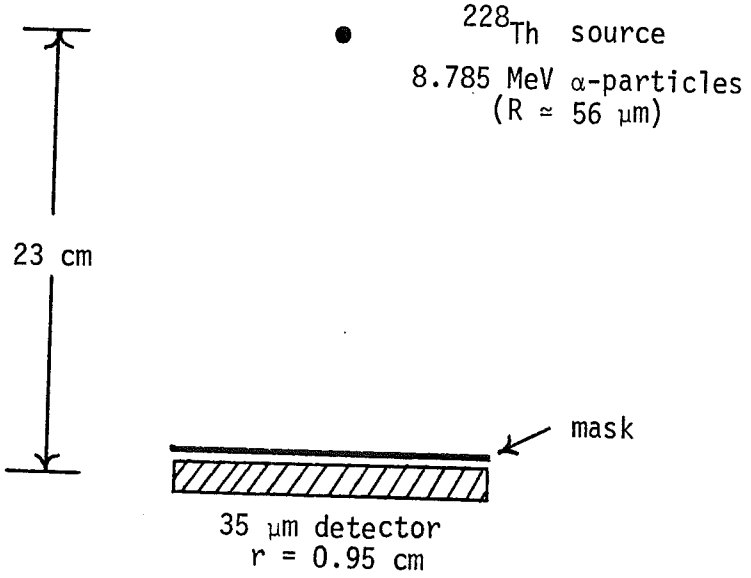

b)

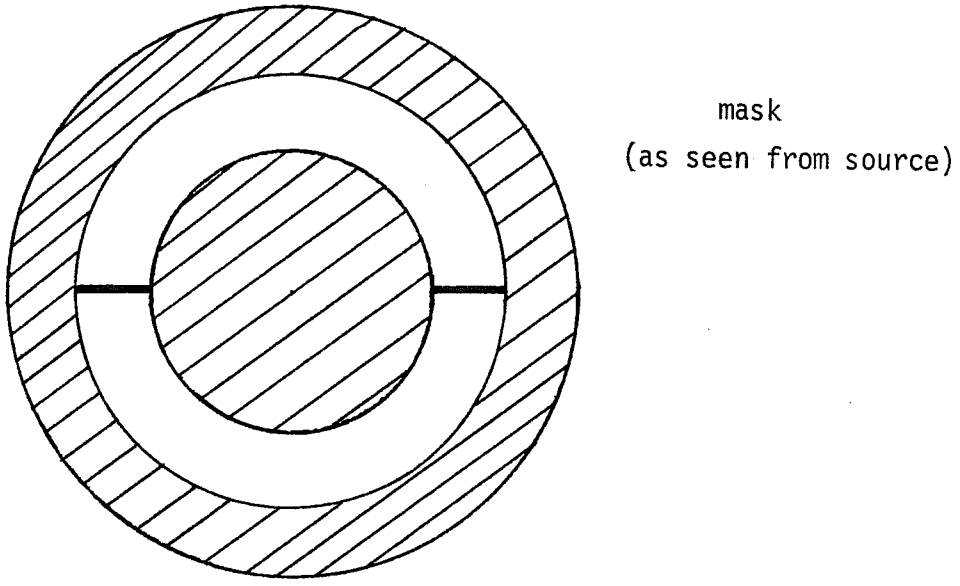

Figure II-2

a)

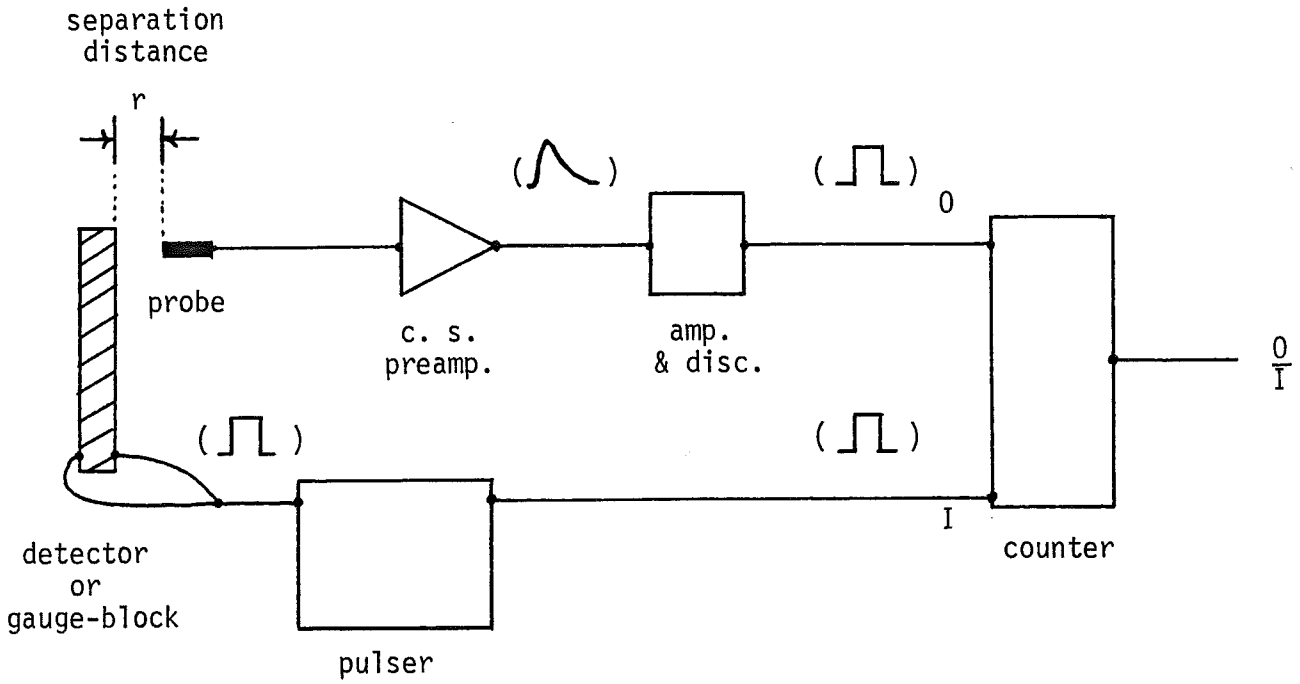

b)

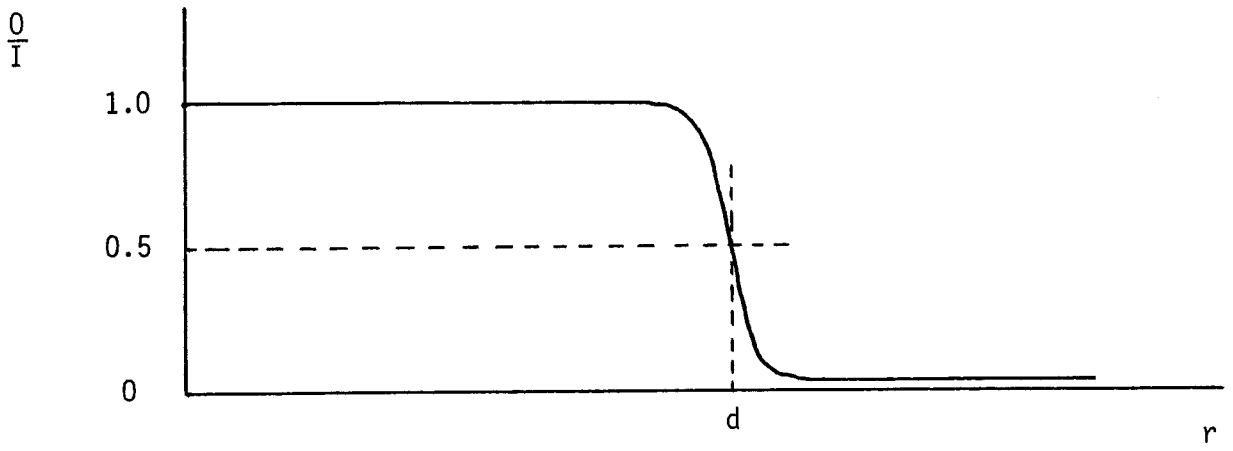

Figure III-1

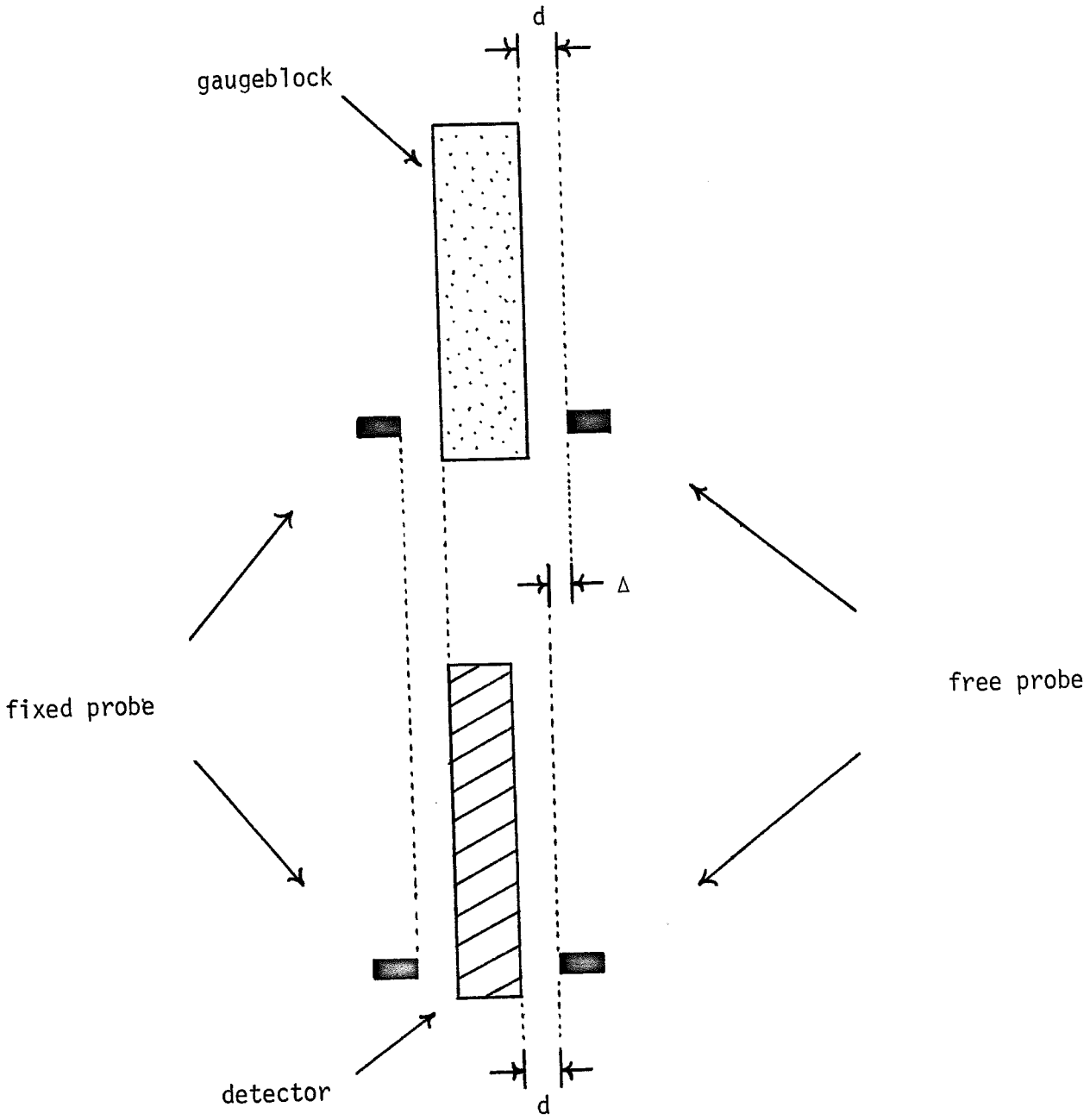

Figure III-2

a)

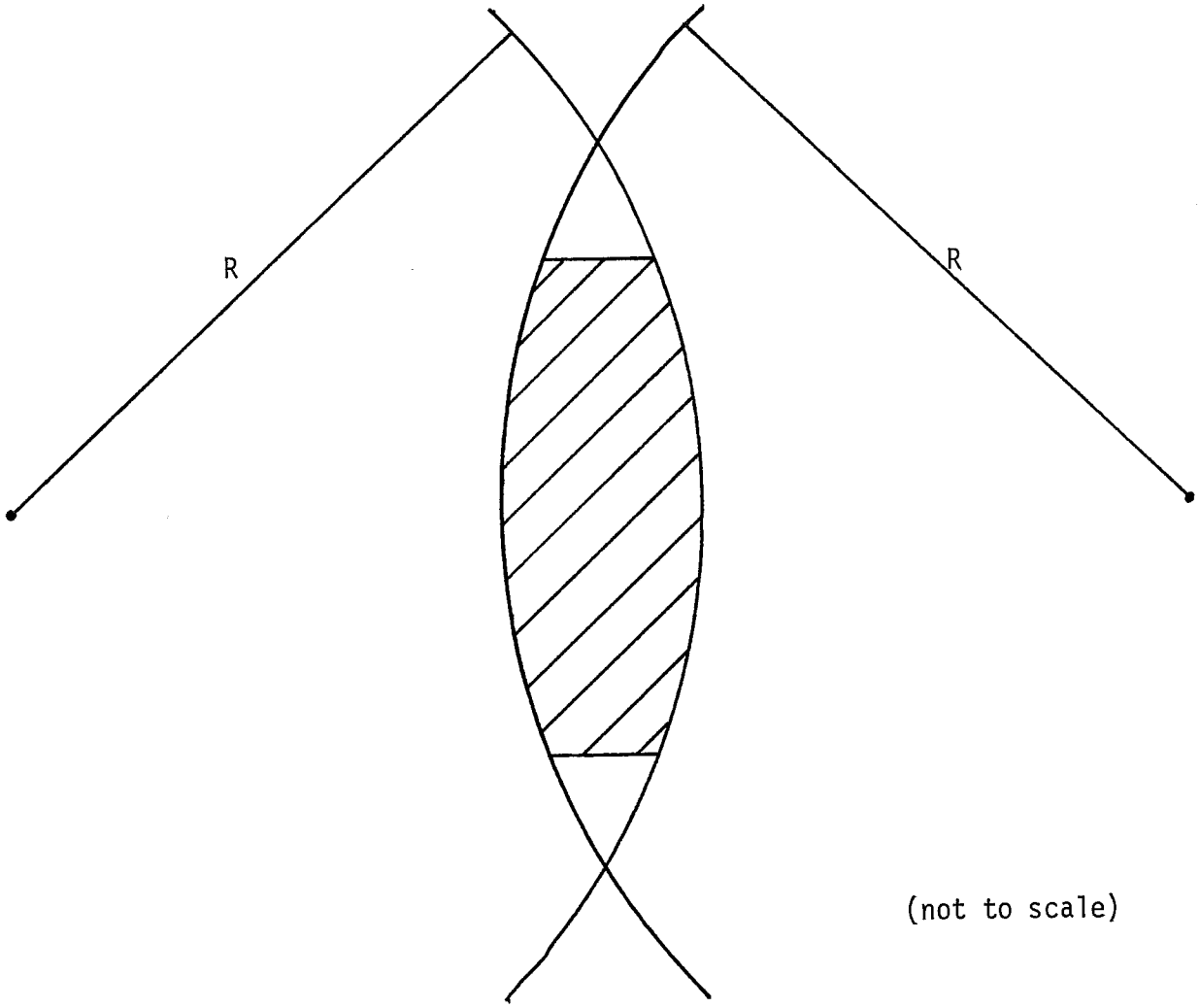

(not to scale)

b)

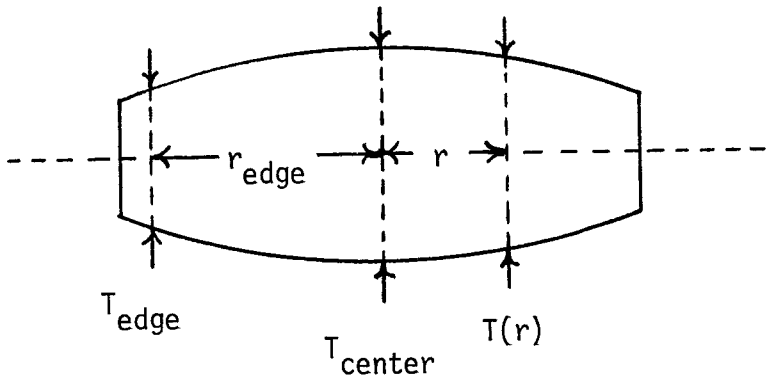

r_{edge} = 8 mm

typically:

T_{center} = 450 µm

T_{edge} = 420 µm

Figure III-3

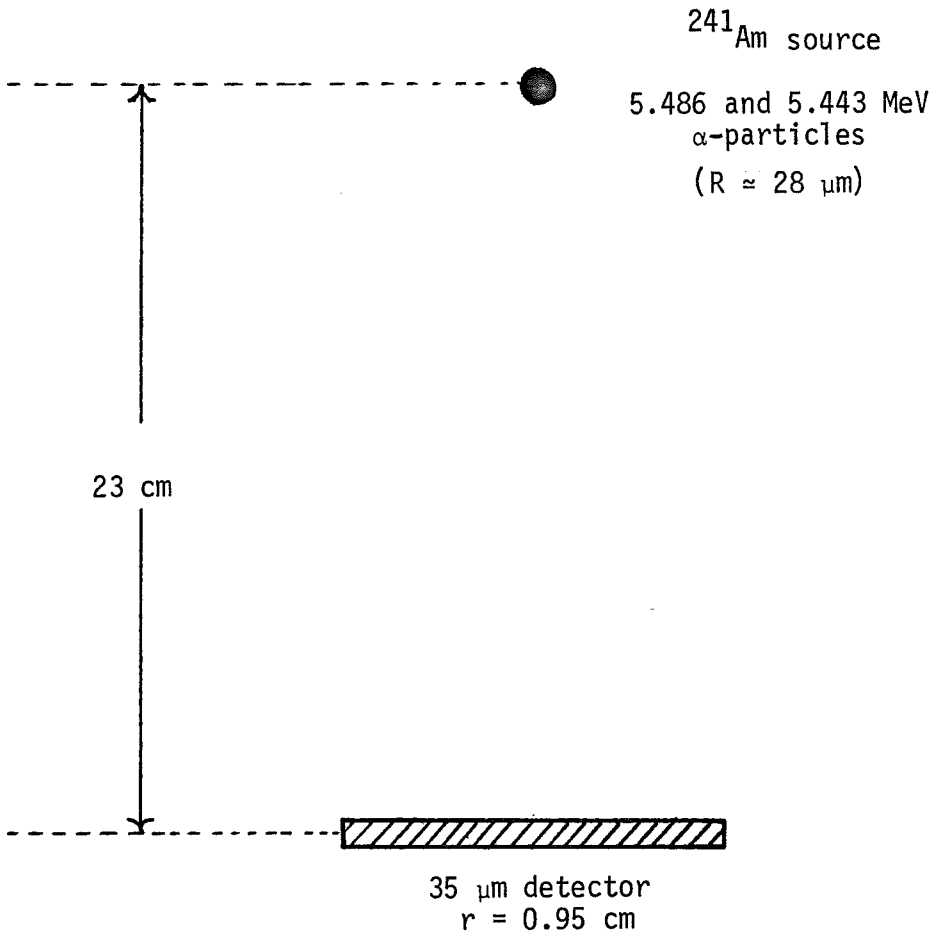
^{241}Am source
5.486 and 5.443 MeV
α-particles
(R ≃ 28 μm)
23 cm
35 μm detector
r = 0.95 cm

Figure IV-1

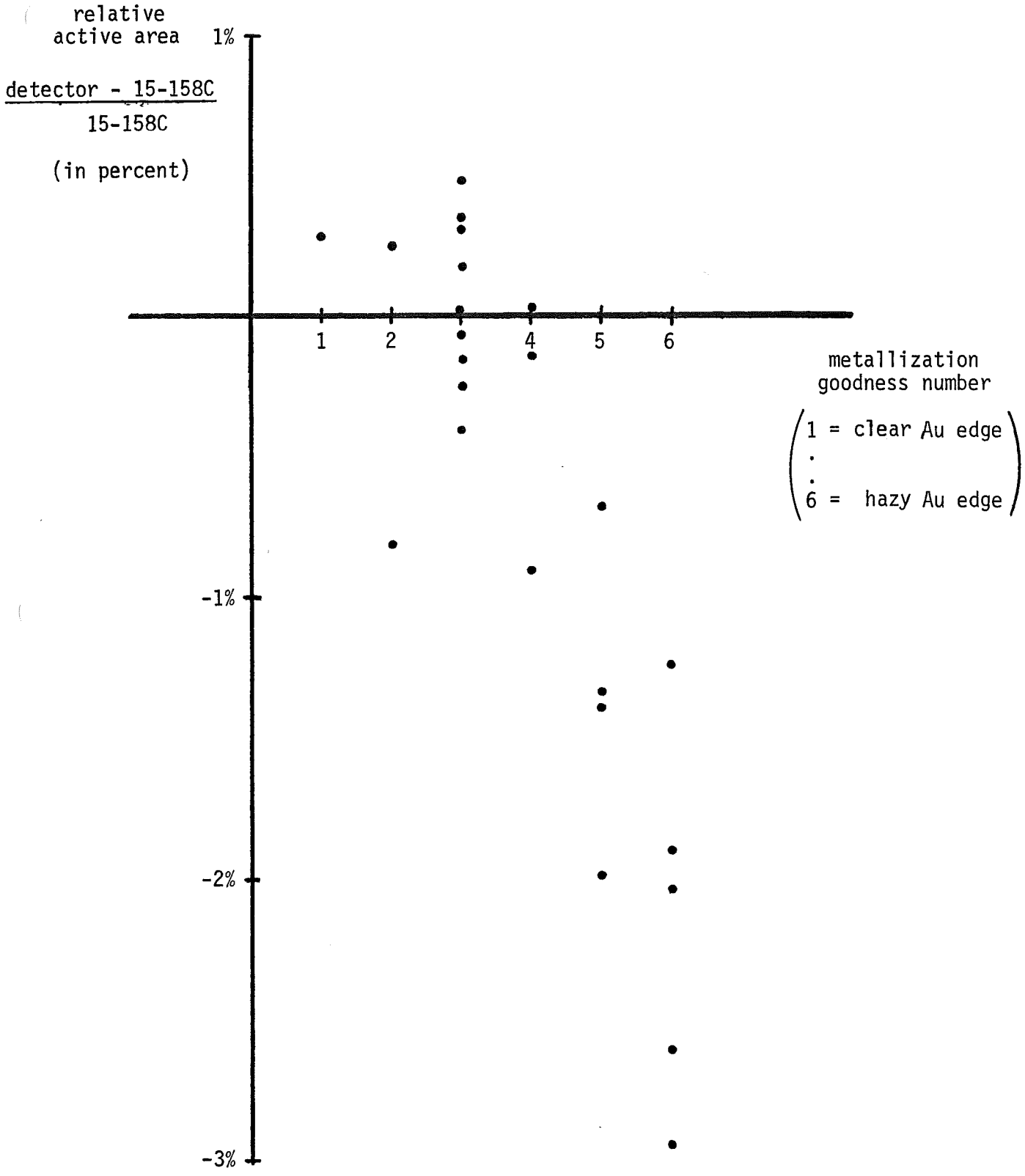
relative
active area
detector - 15-158C
15-158C
(in percent)
1%
-1%
-2%
-3%
1
2
4
5
6
metallization
goodness number
1 = clear Au edge
6 = hazy Au edge

Figure IV-2

a)

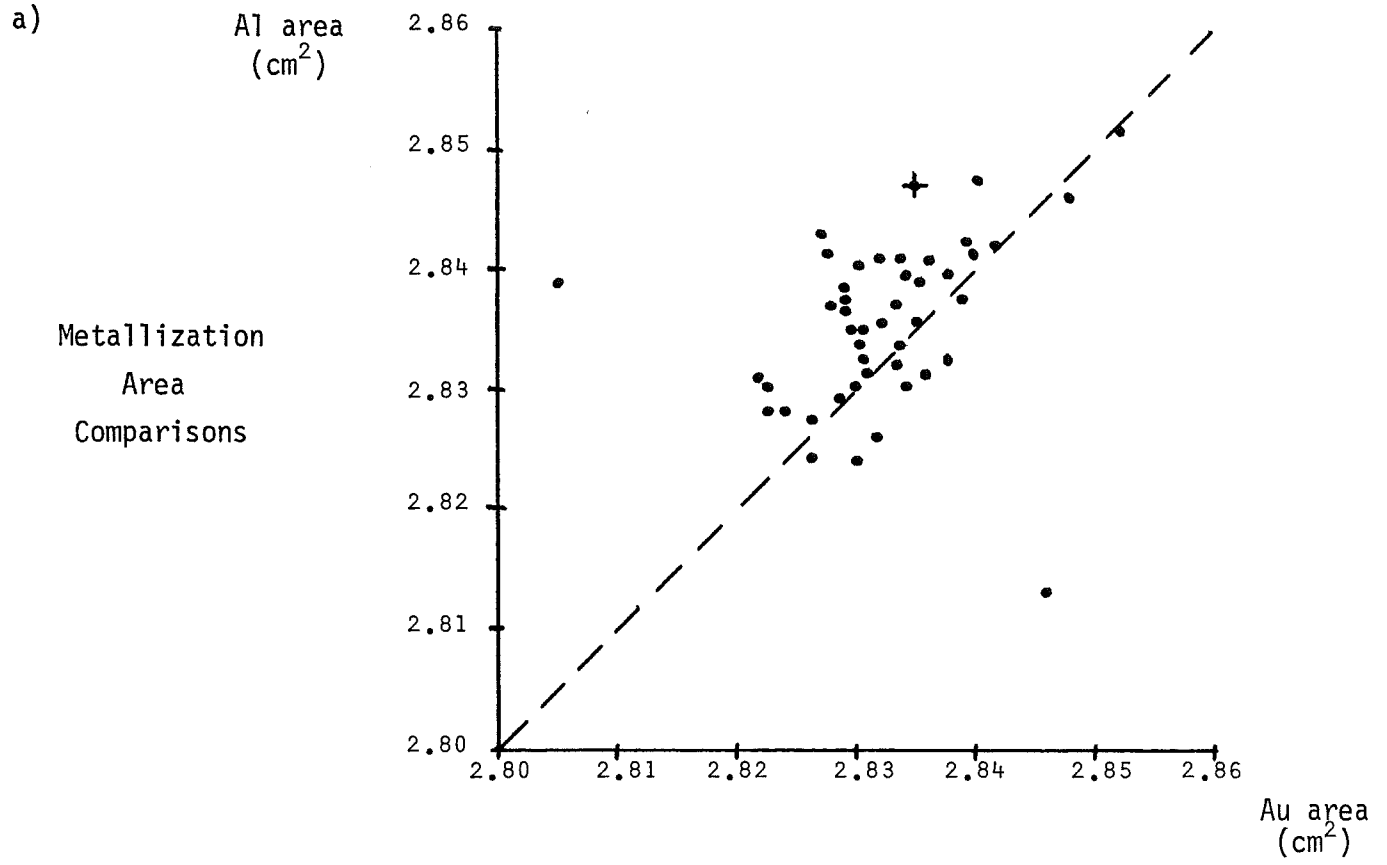

Metallization
Area
Comparisons

b)

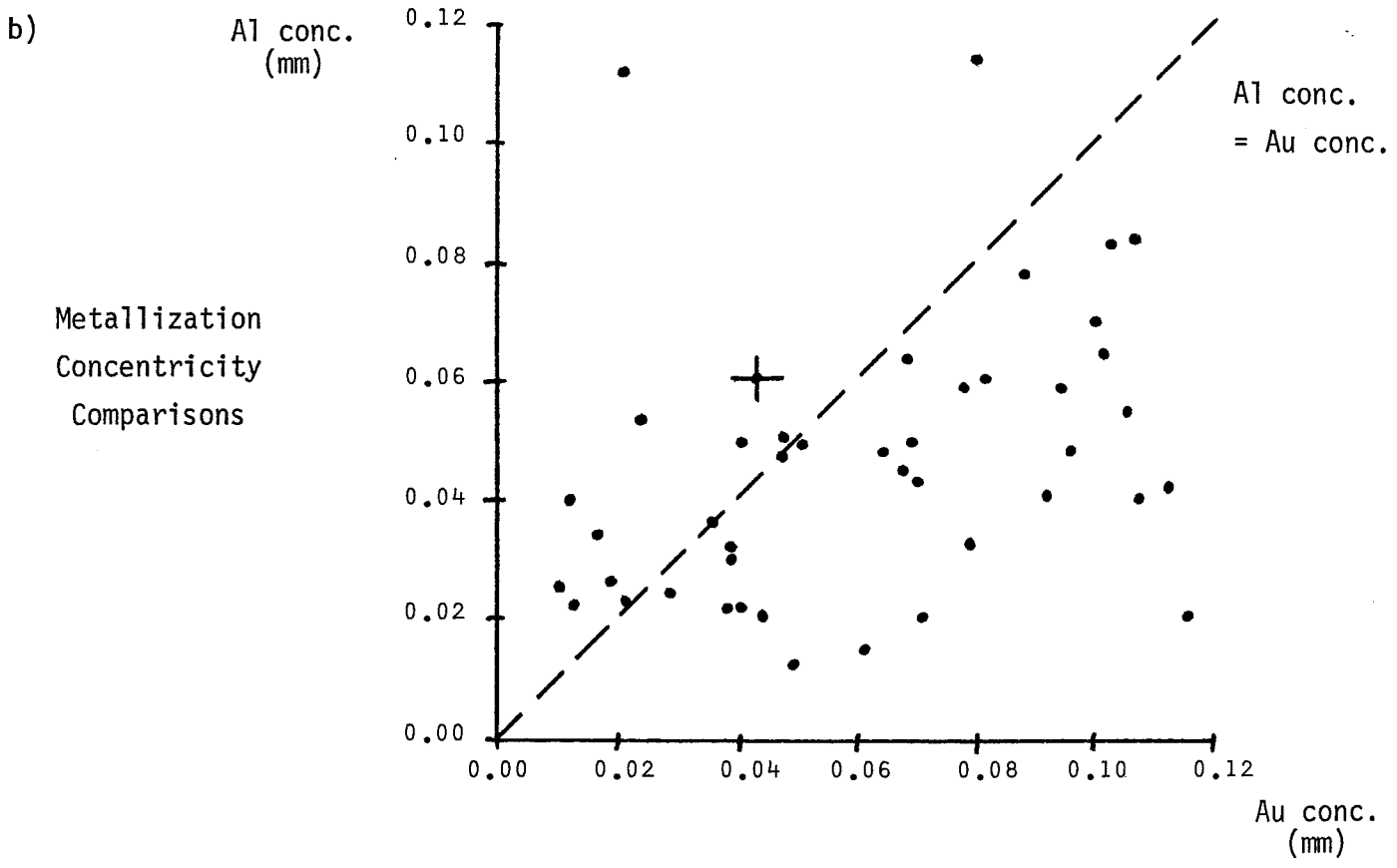

Metallization
Concentricity
Comparisons

Figure V-1